International Journal of Thermophysics, Vol. 20, No. 3, 1999

Nonequilibrium Molecular Dynamics Simulations of Coupled Heat and Mass Transport in Binary Fluid Mixtures in Pores[1]

I. Wold[2] and B. Hafskjold[2, 3]

Molecular dynamics simulations were carried out for a binary fluid mixture in a slit pore. The fluid was an argon-like Lennard–Jones/spline model. The pore wall was represented by the Steele model for a layered graphite structure. The pore had a heat source in one end and a heat sink in the other, resulting in a lateral temperature gradient, a Soret effect, and a thermal creep flow along the pore wall. Potential models with various depths were used to examine the effect of wetting and adsorption on the thermal creep flow. The main results were as follows. (a) A relatively strong creep flow was generated parallel to the wall by the temperature gradient. For strongly attracting fluid–wall potentials, the flow occurred from the cold to the hot end of the pore near the wall (except for the very narrow pore) and oppositely in the center of the pore. For a purely repulsive potential, the flow was weak and mostly in the opposite direction. (b) The thermal diffusion coefficient was comparable to that in bulk fluid at the same overall density, except when the creep flow was strong, in which case the thermal diffusion was blurred by the convective mixing.

KEY WORDS: microporous; nonequilibrium molecular dynamics; slit pore; surface tension; thermal creep; thermal diffusion.

1. INTRODUCTION

In a porous system, it is well known that the thermodynamic properties, such as the phase behavior, may deviate very much from the properties of the bulk fluid. Much less is known about the transport properties, in particular, about coupled transport processes such as coupled heat and mass

[1] Paper presented at the Thirteenth Symposium on Thermophysical Properties, June 22–27, 1997, Boulder, Colorado, U.S.A.

[2] Department of Physical Chemistry, Norwegian University of Science and Technology, N-7034 Trondheim, Norway.

[3] To whom correspondence should be addressed.

0195-928X/99/0500-0847$16.00/0

transport. Thermal creep flow may, however, play a role when normal convection is lacking (under zero gravity), when the system has been established over a long time (hydrocarbon reservoirs subject to the geothermal gradient), or when the thermal force is extremely large.

In most cases, it is very difficult to describe thermal creep, and for that matter, almost any transport process, in a porous material due to the complexity of the pore structure. Most studies based on computer simulations have therefore been made for a pore model with simple geometry, notably for slit pores [1]. The studies of transport phenomena include diffusion, which depends only on the fluid particles and the fluid–wall interactions [1]. Thermal conduction depends, in addition, on the matrix and is, therefore, a more difficult problem, from both a phenomenological and a computational point of view. In this paper, we study thermal diffusion (the Soret effect), i.e., the diffusive process driven by a temperature gradient in a slit pore by nonequilibrium molecular dynamics (NEMD) simulations, and it turns out that this study is feasible and illuminating for very small pores (less than 10 nm pore width). Both wetting and nonwetting interfaces were used.

The boundary-driven NEMD technique has proved to be an accurate and effective method to determine the "cross-coefficients" in coupled transport processes, such as the Soret and Dufour coefficients in coupled heat and mass transport [2, 3]. Several studies have been carried out for thermal diffusion, in particular for isotope mixtures, and we now begin to understand at least the sign of the effect, i.e., which of the components will be driven toward the hot side of the system for a given temperature gradient. Generally for a binary mixture, the component with the higher molecular weight will tend to move to the cold side of the system. For two components with the same molecular weight, the most strongly interacting component will move to the cold side.

This paper describes a study on a model of Lennard–Jones/spline (LJ/s) particles in a slit pore where the pore width and the interaction between the fluid particles and the wall are the main variables. The details of the model and simulation conditions are given in Section 2. Section 3 describes how the thermal diffusion factor and the mass fluxes in the pore depend on these variables. A possible explanation of the thermal creep flow is given in terms of the fluid–wall interfacial tension.

2. MODEL AND SIMULATION CONDITIONS

2.1 Simulation Cell and Potential Models

The simulations were carried out in a noncubic simulation cell with walls at the top and bottom (perpendicular to the z-axis). The general

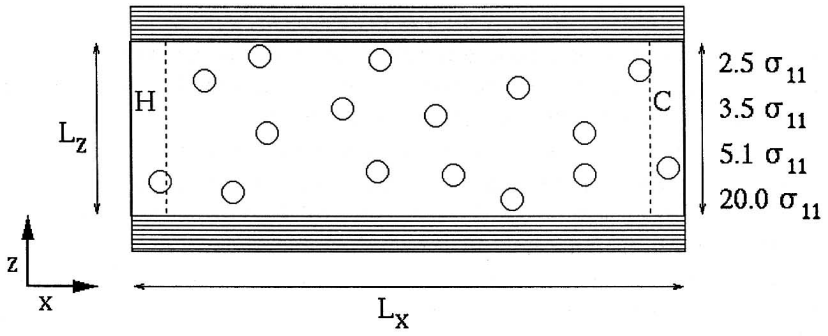

Fig. 1. Layout of the nonequilibrium molecular dynamics simulation cell.

layout of the simulation cell is shown in Fig. 1. The cell was divided into 200 control volumes that extended over the entire MD cell in the y-direction, and organized as 20×10 or 10×20 in the xz-plane; the widest pore had the highest number of layers in the z-direction. The system was locally thermostatted to constant temperatures in regions at each end of the cell, marked H and C in Fig. 1, creating a temperature gradient in the x-direction.

The fluid–fluid and fluid–wall interactions were modeled with the LJ/s potential [4] and the Steele 10–4–3 (10–4–3) potential [5], respectively. The LJ/s potential is defined by

$$\varphi_{ij}(r) = \begin{cases} 4\varepsilon_{ij}\left[\left(\dfrac{\sigma_{ij}}{r}\right)^{12} - \left(\dfrac{\sigma_{ij}}{r}\right)^{6}\right] & \text{for } r \leqslant r_s \\ a_{ij}(r-r_c)^2 + b_{ij}(r-r_c)^3 & \text{for } r_s \leqslant r \leqslant r_c \\ 0 & \text{for } r \geqslant r_c \end{cases} \tag{1}$$

where $r_s = (26/7)^{1/6}\,\sigma_{ij}$, $r_c = (67/48)\,r_s$, $a_{ij} = -(24192/3211)\,\varepsilon_{ij}/r_s^2$, and $b_{ij} = -(387072/61009)\,\varepsilon_{ij}/r_s^3$. The parameters σ_{ij} and ε_{ij} represent the molecular diameters and intermolecular potential depths, respectively. The 10–4–3 potential is defined by

$$\varphi_{sf}(z) = 2\pi\rho_s\varepsilon_{sf}\sigma_{sf}^2\Delta\left[\frac{2}{5}\left(\frac{\sigma_{sf}}{z}\right)^{10} - \left(\frac{\sigma_{sf}}{z}\right)^{4} - \frac{\sigma_{sf}^4}{3\Delta(0.61\Delta + z)^3}\right] \tag{2}$$

where ρ_s is the particle density of the graphite lattice, ε_{sf} and σ_{sf} are the potential parameters equivalent to the Lennard–Jones potential, Δ is a parameter representing the distance between the graphite layers considered in the original development of the model [5], and z is the distance from one of the walls to a fluid particle. In the present study, the fluid particles interact with two walls, and the fluid–wall potential energy is a superposition of two contributions of the type given by Eq. (2). A wall interacting with the fluid through the repulsive WCA modification of the 10–4–3 potential, i.e., the 10–4–3 potential shifted upwards with the potential depth and truncated at the minimum, was also used.

Since the 10–4–3 potential is a function of wall distance only, and independent of x and y, the particle velocities parallel to the wall (the x- and y-components) would be unaffected by collisions with the wall. This corresponds to a system with perfect slip conditions. To reduce the effects of perfect slip and to include the effects of a thermostatted wall, the method of diffuse fluid–wall collisions [1] was used as follows. The system was monitored for fluid–wall collisions. When a collision between a fluid particle and the wall was detected as a change in sign of the z-component of the particle velocity, the particle was given new velocity components in the x- and y-directions, drawn from a Maxwell–Boltzmann distribution corresponding to the local wall temperature. The z-component was given by the unperturbed equations of motion.

2.2. Simulation Conditions

Four pore widths were studied: 2.5, 3.5, 5.1, and 20.0 molecular diameters. The fluid–fluid interaction parameters were argon-like, and the fluid–wall interaction was modeled with the cross parameters of argon and carbon. In addition, the fluid–wall interaction strength was reduced to ~ 30 and $\sim 14\%$ of the full value. The reduction of the interaction strength was done to reduce the adsorption and make a softer wall repulsion. The simulation conditions are given in terms of the potential parameters in Table I.

The full 10–4–3 fluid–wall attraction at the potential minimum is stronger than the fluid–fluid interaction by a factor between 9 and 12, depending on the pore width. The smaller pores exhibit a deeper potential minimum due to increasing influence from the opposite wall.

The simulations were run between 1.2×10^6 and 1.8×10^6 time steps, of which the last 1.0×10^6 to 1.6×10^6 time steps were used for analysis, leaving 0.2×10^6 time steps for a steady state to be established. The analysis of the NEMD data was based on accumulated data dumped every 50,000 or 60,000 time steps, depending on the system.

Table I. Potential Parameters and Simulation Conditions

Quantity	Symbol	Value
Molecular size parameter[a]	σ	0.341 nm
Potential well-depth parameter[a]	ε/k_B	118.9 K
Fluid–wall size parameter	σ_{sf}	0.3405 nm
Fluid–wall potential well-depth parameter	ε_{sf}/k_B	57.9 K
Reduced fluid–wall potential well-depth parameter 1	ε_{sf}/k_B	17.9 K
Reduced fluid–wall potential well-depth parameter 2	ε_{sf}/k_B	7.9 K
Density of C atoms in wall	ρ_s	114 nm^{-3}
Separation of graphite layers	Δ	0.335 nm
Component mass ratio	m_1/m_2	10
Overall fluid density[b]	ρ	10 nm^{-3}
Temperature at hot pore end, thermostat set point	T_H	240 K
Temperature at cold pore end, thermostat set point	T_C	120 K

[a] The two fluid components had the same values for σ and ε and differed only by mass.
[b] This value is nominal based on the wall position. The actual particle number density in the pore is higher, especially for the narrow pores, due to the excluded volume near the walls.

3. RESULTS

3.1. Concentration Gradients and Thermal Diffusion Factors

During the initial simulation period, in which a steady state was established with a given temperature gradient, the thermal diffusion created a stable concentration gradient. From these gradients we calculated the thermal diffusion factor, defined by

$$\alpha_{12} = -\left(\frac{T\,\nabla x_1}{x_1 x_2\,\nabla T}\right)_{J_1 = J_2 = 0} \tag{3}$$

for the two-component system, where x_1 and x_2 are the molar fractions of species 1 and 2, respectively. The subscript signifies that the two diffusive mass fluxes must be zero for this definition to apply. Table II shows that the thermal diffusion factor varies as functions of both pore size and potential. The high α_{12} values seen for the smaller pores are partly explained by the high actual densities in these pores, because the thermal diffusion factor increases with increasing density. The very low α_{12} seen for the widest pore may seem somewhat surprising, given that one expects the value of α_{12} to approach the bulk value, ~ 1.0, when the pore width increases. However, there are local fluxes that tend to mix the contents of the pore (see Section 3.2). This mixing occurs in the wide pores, but not in the narrow ones.

Table II. The Thermal Diffusion Factor α_{12}, at $T = 180$ K for $\rho = 10\ \text{nm}^{-3}$ and Diffuse Walls

		10–4–3	WCA
Pore width	Pot. param.[a]	α_{12}	α_{12}
2.5σ	Full	1.5 ± 0.1	1.6 ± 0.1
	Reduced 1	1.8 ± 0.2	1.7 ± 0.3
	Reduced 2	1.5 ± 0.2	1.9 ± 0.2
3.5σ	Full	1.0 ± 0.1	1.5 ± 0.1
	Reduced 1	1.6 ± 0.1	1.8 ± 0.1
	Reduced 2	1.6 ± 0.1	1.7 ± 0.1
5.1σ	Full	0.8 ± 0.1	1.5 ± 0.1
	Reduced 1	1.5 ± 0.1	1.5 ± 0.1
	Reduced 2	1.5 ± 0.1	1.5 ± 0.1
20.0σ	Full	0.0 ± 0.1	0.3 ± 0.1
	Reduced 1	0.4 ± 0.1	
	Reduced 2	0.4 ± 0.1	

[a] The potential parameters refer to the potential parameters given in Table I for the wall–fluid interaction. The WCA is constructed from the corresponding 10–4–3 potential as described in the text.

Even though the average mass flux over the entire pore is zero as required by the definition, Eq. (3), the local mixing will reduce the computed estimate of α_{12}. Since there is a nonzero flux over the spatial region used for the computation of α_{12}, one may argue that the condition of zero mass fluxes in Eq. (3) is not fulfilled for the wide pores.

3.2. Mass Flux

The simulation cell is closed at each end, and the net mass flux in the x-direction has to be equal to zero. This does not prevent significant internal mass fluxes local to parts of the cell. When the mass flux in the x-direction, parallel to the heat flux, is plotted as a function of z, some characteristic flow patterns appear. This flow is best seen in the pores of width 5.1σ and 20σ, and these are shown as examples in Figs. 2 and 3. A negative flux in these figures signifies a mass flux from cold to hot, or from right to left in Fig. 1.

The two-dimensional projection of the flow vectors for the pore of width 20σ in Fig. 4, shows the flow even more clearly. This flow pattern explains the low α_{12} for the 20σ and 5.1σ pores as shown in Table II, as

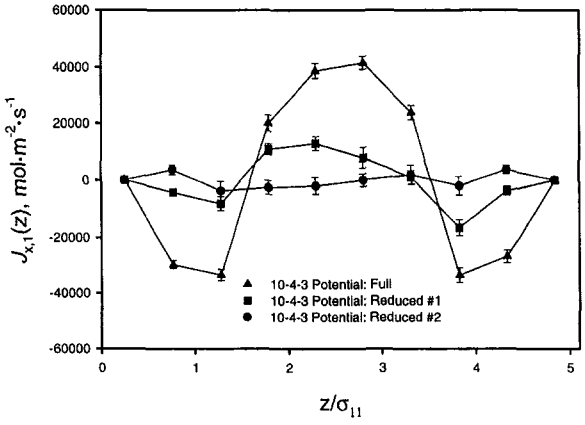

Fig. 2. Mass flux parallel to the wall as a function of the distance from the wall for the 5.1σ pore with various attractive potentials.

it inhibits the formation of a large concentration gradient. It also explains why α_{12} is lowest for the full potential, as the flow is largest here.

3.3. Interfacial Tension

It was anticipated that the driving force behind the observed vortices within the systems was the interaction between the fluid particles and the

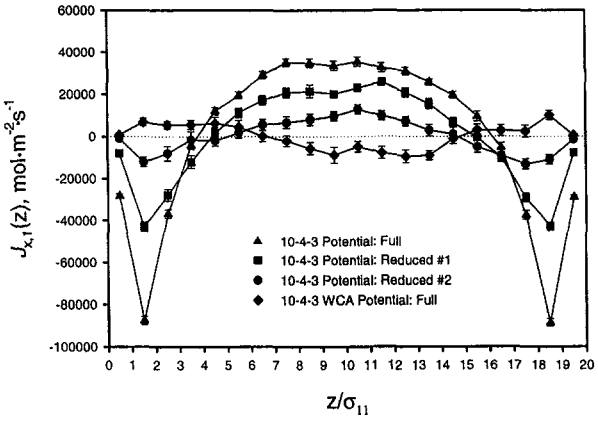

Fig. 3. Mass flux parallel to the wall as a function of the distance from the wall for the 20σ pore with various attractive potentials.

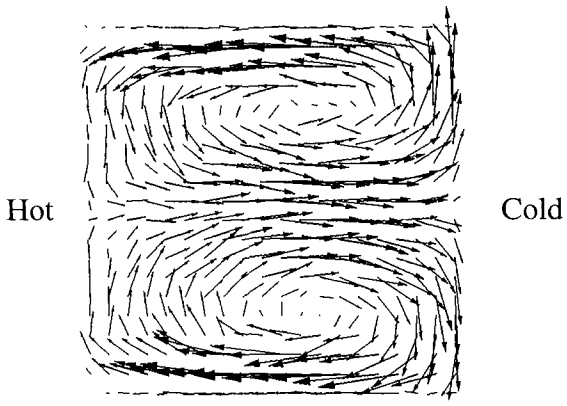

Fig. 4. Two-dimensional (x, z-projection) flow pattern in the 20σ simulation cell.

wall, in combination with the temperature gradient. Another possible explanation we considered, was the increased kinetic energy and consequent increased pressure at the hot side as compared to the cold side. This explanation was eventually ruled out because it would lead to increased fluxes when the fluid–wall interaction decreased, whereas the opposite dependency was observed.

It is known that a gradient in surface tension will cause a mass flow, the so-called Marangoni effect. The question here was if the temperature gradient could cause a gradient in the fluid–wall interfacial tension to act like a "thermal Marangoni effect." The fluid–wall interfacial tension gradient, $\nabla\gamma_{sf}$, was computed and is given in Table III along with values of the significant wall mass flux.

The term "significant wall mass flux" and the problems and sorting criteria shall be explained, as determining the direction of the mass flux along the wall is not always a simple task. The wall is used as a reference because the fluid–wall interfacial tension works close (and parallel) to the wall.

If the pore is narrow, the counterflow in the center of the pore may virtually cancel the wall flow at this wall due to viscous forces. This is why no distinct vortex was observed in the narrow pores. In cases of small gradients in the interfacial tension, it was usually found that only the colder part of the pore sustains two symmetric vortices, like those shown in Fig. 4, except shifted toward the cold part of the pore. The hot part exhibits essentially no flow in such cases. When the diffuse wall condition was used, velocities centered at zero x- and y-components were assigned to the particles after collision with the wall, leading to very small mass fluxes

Table III. Surface Tension Gradients and Significant Wall Mass Flux

		10–4–3 potential		WCA potential	
Pore	ε_{sf}/k_B [a]	$\nabla\gamma$ (10^6 N·m^{-2})	J_M (10^3 mol·m^{-2}·s^{-1})[b]	$\nabla\gamma^*$ (10^6 N·m^{-2})	J_M (10^3 mol·m^{-2}·s^{-1})[b]
2.5σ	Full	4.4 ± 0.1	20 ± 3	3.6 ± 0.1	15 ± 2
	Reduced 1	6.4 ± 0.2	16 ± 3	6.5 ± 0.2	16 ± 3
	Reduced 2	8.4 ± 0.2	11 ± 3	8.5 ± 0.2	11 ± 3
3.5σ	Full	-6.9 ± 0.1	-7.7 ± 0.3	-1.32 ± 0.05	ns[c]
	Reduced 1	-1.1 ± 0.05	ns	-0.15 ± 0.05	ns
	Reduced 2	0.6 ± 0.1	ns	0.68 ± 0.05	ns
5.1σ	Full	-7.4 ± 0.1	-30 ± 1	1.05 ± 0.05	5.47 ± 0.08
	Reduced 1	-1.33 ± 0.05	-4 ± 1	0.88 ± 0.05	5 ± 1
	Reduced 2	-0.52 ± 0.05	4 ± 2	—	—
20σ	Full	-15.0 ± 0.2	-28.22 ± 0.09	0.14 ± 0.05	0.8 ± 0.2
	Reduced 1	-1.6 ± 0.1	-7.9 ± 0.8	—	
	Reduced 2	-0.44 ± 0.05	-0.8 ± 0.4	—	

[a] See Table I, footnote *a*.

[b] The numbers reported here are for the control volume nearest to the wall, such that the mass flux in the control volume is nonzero. See text for a further explanation of "significant wall mass flux."

[c] Not significant.

near the wall. The control volumes nearest to the wall in the narrowest pore were influenced by this, as shown in Fig. 2. The term "significant wall mass flux" is therefore used in those cases where the mass flux clearly shows vortices, and it signifies the maximum in the x-component of the mass flux, considered as function of z. A visual inspection of the flow vectors like those in Fig. 4 can be used to determine if, for example, the hot part has a chaotic pattern that masks the flow pattern of the cold part in the analysis.

The observed linear relationship between the gradient in interfacial tension and the significant mass flux, given in Table III, is consistent with the explanation that the flux is driven by the gradient in interfacial tension. Note also that the dependency of the gradient in interfacial tension on the fluid–wall interaction points to the same explanation; when the interaction is changed from attractive (wetting) to repulsive (non-wetting), the gradient in interfacial tension and the significant mass flux change sign in most cases.

We expect that using a corresponding system with specular wall conditions would more clearly (but less realistically) show the thermal creep flow.

4. CONCLUSIONS

We have shown that two vortices are generated in a closed slit pore when the pore is subject to a temperature gradient along the parallel walls. Two possible explanations were considered: (1) the pressure is higher in the hot part of the pore than in the cold, and (2) the gradient in the fluid–wall interfacial tension drives a creep flow along the wall. The flow occurred in the direction from low to high interfacial tension, which is from cold to hot in most of the cases studied here. In the larger pores with purely repulsive fluid–wall interactions, the flow occurred from hot to cold near the wall, but this was also from low to high interfacial tension. On this basis, we conclude that the flow was generated by the gradient in interfacial tension. The effect is therefore characterized as a thermal Marangoni effect.

The thermal diffusion factor is of the same order of magnitude in the slit pore as in bulk fluid, but the component separation due to thermal diffusion is blurred in the cases with strong local currents.

REFERENCES

1. R. F. Cracknell, D. Nicholson, and K. E. Gubbins, *J. Chem. Soc. Faraday Trans.* **91**:1377 (1995).
2. J. M. Kincaid and B. Hafskjold, *Mol. Phys.* **82**:1099 (1994).
3. J. M. Simon, *Étude de la thermodiffusion dans des mélanges fluides de n-alcanes par simulation numérique de la dynamique moléculaire*, Ph.D. thesis (Université de Paris Sud, Paris, 1997).
4. B. L. Holian and D. J. Evans, *J. Chem. Phys.* **78**:5147 (1983).
5. W. A. Steele, *The Interaction of Gases with Solid Surfaces* (Pergamon, Oxford, 1974), Chap. 2.